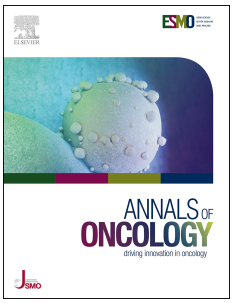

Deep learning radiomic nomogram can predict the number of lymph node metastasis in locally advanced gastric cancer: an international multi-center study

D. Dong, M.-J. Fang, L. Tang, X.-H. Shan, J.-B. Gao, F. Giganti, R.-P. Wang, X. Chen, X.-X. Wang, D. Palumbo, J. Fu, W.-C. Li, J. Li, L.-Z. Zhong, F. De Cobelli, J.-F. Ji, Z.-Y. Liu, J. Tian

PII: S0923-7534(20)39294-2

DOI: https://doi.org/10.1016/j.annonc.2020.04.003

Reference: ANNONC 154

To appear in: *Annals of Oncology*

Received Date: 22 October 2019

Revised Date: 11 March 2020

Accepted Date: 6 April 2020

Please cite this article as: Dong D, Fang MJ, Tang L, Shan XH, Gao JB, Giganti F, Wang RP, Chen X, Wang XX, Palumbo D, Fu J, Li WC, Li J, Zhong LZ, De Cobelli F, Ji JF, Liu ZY, Tian J, Deep learning radiomic nomogram can predict the number of lymph node metastasis in locally advanced gastric cancer: an international multi-center study *Annals of Oncology* (2020), doi: https://doi.org/10.1016/j.annonc.2020.04.003.

Deep learning radiomic nomogram can predict the number of lymph node metastasis in locally advanced gastric cancer: an international multi-center study

Authorship:

D. Dong[1,2#], M.-J. Fang[1,2#], L. Tang[3#], X.-H. Shan[4#], J.-B. Gao[5#], F. Giganti[6,7,8#], R.-P. Wang[9], X. Chen[10,11], X.-X. Wang[4], D. Palumbo[8,12], J. Fu[3], W.-C. Li[9], J. Li[5], L.-Z. Zhong[1,2], F. De Cobelli[8,12], J.-F. Ji[13*], Z.-Y. Liu[10*], J. Tian[1,14,15*]

[#]these authors contributed equally to this work.

Affiliations:

[1] CAS Key Laboratory of Molecular Imaging, Institute of Automation, Chinese Academy of Sciences, Beijing, China

[2] School of Artificial Intelligence, University of Chinese Academy of Sciences, Beijing, China

[3] Key Laboratory of Carcinogenesis and Translational Research (Ministry of Education/Beijing), Radiology department, Peking University Cancer Hospital & Institute, Beijing, China

[4] Department of Radiology, Affiliated People's Hospital of Jiangsu University, Zhenjiang, Jiangsu, China

[5] Department of Radiology, The First Affiliated Hospital of Zhengzhou University, Zhengzhou, Henan, China

[6] Department of Radiology, University College London Hospital NHS Foundation Trust, London, UK

[7] Division of Surgery and Interventional Science, Faculty of Medical Sciences, University College London, London, UK

[8] Department of Radiology, Experimental Imaging Centre, San Raffaele Scientific Institute, Milan, Italy

[9] Department of Radiology, Guizhou Provincial People's Hospital, Guiyang, Guizhou, China

[10] Department of Radiology, Guangdong Provincial People's Hospital/Guangdong Academy of Medical Sciences, Guangzhou, Guangdong, China

[11] Department of Radiology, Guangzhou First People's Hospital, Guangzhou, Guangdong, China

[12] Vita-Salute San Raffaele University, Milan, Italy

[13] Key Laboratory of Carcinogenesis and Translational Research (Ministry of Education/Beijing), Gastrointestinal Cancer Center, Peking University Cancer Hospital & Institute, Beijing, China

[14] Beijing Advanced Innovation Center for Big Data-Based Precision Medicine, School of Medicine, Beihang University, Beijing, China

[15] Engineering Research Center of Molecular and Neuro Imaging of Ministry of Education, School of Life Science and Technology, Xidian University, Xi'an, Shaanxi, China

***Correspondence to:**

Prof. Jie Tian

CAS Key Laboratory of Molecular Imaging, Institute of Automation, Chinese Academy of Sciences, No. 95 Zhongguancun East Road, Hai Dian District, Beijing 100190, China.

Tel: +86-10-82618465;

Email: jie.tian@ia.ac.cn

Prof. Zai-Yi Liu

Guangdong Provincial People's Hospital/Guangdong Academy of Medical Sciences, No.106 Zhongshan Er Road, Guangzhou 510080, China

Tel: +86-20-83870125;

E-mail: zyliu@163.com

Prof. Jia-Fu Ji

Key Laboratory of Carcinogenesis and Translational Research (Ministry of Education/Beijing), Gastrointestinal Cancer Center, Peking University Cancer Hospital & Institute, No. 52 Fu Cheng Road, Hai Dian District, Beijing 100142, China.

Tel: +86-10-88196598;

E-mail: jijiafu@hsc.pku.edu.cn

Running Head: Deep learning radiomic nomogram for N staging in locally advanced gastric cancer

Word count: 3841

Abstract

Background

Preoperative evaluation of the number of lymph node metastasis (LNM) is the basis of individual treatment of locally advanced gastric cancer (LAGC). However, the routinely used preoperative determination method is not accurate enough.

Patients and methods

We enrolled 730 LAGC patients from 5 centers in China and 1 center in Italy, and divided them into 1 primary cohort, 3 external validation cohorts, and 1 international validation cohort. A deep learning radiomic nomogram (DLRN) was built based on the images from multi-phase computed tomography (CT) for preoperatively determining the number of LNM in LAGC. We comprehensively tested the DLRN and compared it with three state-of-the-art methods. Moreover, we investigated the value of the DLRN in survival analysis.

Results

The DLRN showed good discrimination of the number of LNM on all cohorts (overall C-indexes: 0.821, 95% CI: 0.785-0.858 in the primary cohort; 0.797, 95% CI: 0.771-0.823 in the external validation cohorts; and 0.822, 95% CI: 0.756-0.887 in the international validation cohort). The nomogram performed significantly better than the routinely used clinical N stages, tumor size, and clinical model ($p<0.05$). Besides, DLRN is significantly associated with the overall survival of LAGC patients (n=271).

Conclusion

A deep learning-based radiomic nomogram had good predictive value for LNM in LAGC. In staging-oriented treatment of gastric cancer, this preoperative nomogram could provide baseline information for individual treatment of LAGC.

Keywords

Lymph node metastasis, Deep learning, Radiomic nomogram, Locally advanced gastric cancer.

Highlights

1) Evaluation of the lymph node metastasis (LNM) is the basis of individual treatment of locally advanced gastric cancer (LAGC);

2) Deep leaning radiomic nomogram (DLRN) based on CT images can preoperatively determine the number of LNM in LAGC;

3) DLRN is significantly superior to the routinely used clinical N stages, tumor size, and clinical model;

4) DLRN is significantly associated with the overall survival of LAGC.

Introduction

Gastric cancer is the third leading cause of death from cancer worldwide[1]. The incidences in Asia, Eastern Europe, and South America are relatively high[2,3].

Locally advanced gastric cancer (LAGC), characterized by wall invasion deeper than the submucosa, is associated with a high rate of lymph node metastasis (LNM) and poor clinical outcomes[4]. According to the 8th American Joint Committee on Cancer (AJCC) TNM staging system, the severity of lymph node (LN) involvement is classified based on the number of LNMs as N0 (no LNM), N1 (1–2 LNMs), N2 (3–6 LNMs), N3a (7–15 LNMs), and N3b (>15 LNMs)[5].

Accurate preoperative N staging is one of the bases of individual treatment of LAGC. Patients with different N stages have significantly different prognosis and may need a different extent of lymphadenectomy or neoadjuvant treatment[4]. The European prospective randomized Dutch trial showed that extended lymphadenectomy (D2) had a superior survival than limited lymphadenectomy (D1) in LAGC patients with N2 stage[6]. The European Society for Medical Oncology (ESMO) and National Comprehensive Cancer Network (NCCN) guidelines recommend preoperative N staging using medical imaging[3-4]. In particular, computed tomography (CT) imaging has been routinely used for preoperative N staging, with enlarged and round-shaped LNs as a sign of LNM[5]. However, the accuracy of CT is approximately 50%–70% for LNM[7], which is unsatisfactory.

Radiomics is an emerging technique that converts standard-of-care medical images into hand-crafted radiomic features and then selects critical features as a signature for quantitative cancer diagnostics[8-11]. Radiomic nomogram, a graphic representation of model that combines radiomic signature and clinical characteristics, has improved the prediction ability of peritoneal metastasis in LAGC[12]. In combination with deep learning features automatically learned from convolutional neural networks, radiomics showed excellent performance in cancer prognosis[13]. However, the use of deep learning radiomics to predict N stages in LAGC has yet to be reported.

To address this, we aimed to develop a deep learning radiomic nomogram (DLRN) for N staging in LAGC. We focused on preoperatively discriminating pathologic N0,

N1, N2, N3a, and N3b, since an accurate staging is the basis of individual treatment.

Patients and Methods

Patients

This retrospective study was approved by the Institutional Review Board of all participating hospitals, and the requirement for informed consent was waived.

Patients were enrolled with the following criteria. Inclusion criteria: (a) pathologically diagnosed as LAGC (pT2-4aNxM0); (b) D2 lymph node dissection with at least 16 LNs during the surgery; (c) CT performed less than 2 weeks before surgery. Exclusion criteria: (a) preoperative therapy (radiotherapy, chemotherapy, or other treatments); (b) previous abdominal malignancies or inflammatory diseases; (c) difficult to segment the tumor because of unsatisfactory gastric distention; (d) artifacts on CT images seriously deteriorating the observation of LNs.

As shown in Figure 1 and Supplementary A1, 679 LAGC patients were enrolled from five centers in China and divided into four cohorts: a primary cohort for training (PC, n=225) and three validation cohorts (VC1, n=178; VC2, n=145; VC3, n=131). An international validation cohort (IVC, n=51) was collected from Italy. Besides, a follow-up cohort (n=271) was used for survival analysis in LAGC.

Clinical characteristics

The clinical characteristics of the patients are shown in Table S1. The gold standard for N stages was pathologically assessed after surgery. The clinical N and clinical T stages were determined based on preoperative CT images by experienced radiologists, according to the 8th AJCC TNM staging system[5,14].

CT imaging

All patients in PC, VC1, and VC2 underwent both unenhanced and biphasic (arterial and venous phase) contrast-enhanced CT before surgery. Patients in VC3 and IVC underwent only biphasic contrast-enhanced CT. The CT image acquisition settings are shown in Supplementary A2 and Table S2.

Procedures

Figure 1 shows the flowchart of this study. The DLRN modeling pipeline is shown

in Figure 2.

Tumor region segmentation

Tumor regions of interest (ROIs) were manually delineated on multi-phase CT images by an experienced radiologist (reader 1). For each CT phase, only one slice with the largest tumor area was chosen visually by the radiologist and a 2-dimensional ROI of the tumor was delineated using ITK-SNAP software (version 3.6.0; http://www.itksnap.org). After 3 months, 30 patients in the PC were randomly selected, and their ROIs were segmented again by reader 1 and another radiologist (reader 2) to construct two re-segmentation datasets for the assessment of intra-/inter-reader reproducibility of radiomic features.

Radiomic feature extraction

A total of 112 deep learning features and 289 hand-crafted features were extracted from each ROI, totaling 1203 features from the three ROIs per patient (Supplementary A3). We adapted the DenseNet-201 architecture to develop our deep convolutional neural networks (DCNNs) for deep learning feature extraction[15]. The hand-crafted features included shape, global texture, and local texture.

Radiomic signature building

Feature selection and signature building were performed in PC (Supplementary A4). Three signatures were respectively built from the three ROIs as follows: 1) Intra-/inter-class correlation coefficients (ICCs) and coefficient of variation (CV) were calculated on the re-segmentation dataset and a simulated slice thickness dataset (Supplementary A5), respectively. The stable features with ICCs>0.8 and CV<15% were selected to adapt different segmentations and different slice thicknesses. 2) The features were divided into several clusters by hierarchical clustering and the most representative medoid feature in each cluster was reserved. 3) Three methods, including support vector machine (SVM), artificial neural network (ANN) and random forest (RF), were compared and the best method was used to construct three predictive signatures.

DLRN construction

Univariate analysis was used to select statistically significant clinical

characteristics ($p<0.05$). Multivariable linear regression analysis was conducted to build the DLRN from the clinical characteristics and radiomic signatures. We mainly considered contrast-enhanced radiomic signatures in our DLRN. But the incremental predictive value of unenhanced radiomic signature to DLRN was also investigated using the net reclassification index (NRI).

The association of DLRN score with pathologic N stages was assessed using the Spearman correlation analysis. Logistic regression was used to predict the probability belonging to each N stage with the DLRN score. Additionally, a classification procedure was proposed based on cutoffs of the logistic regressions above to split patients into subgroups of N stages. Furthermore, multivariable logistic regression was performed to build a clinical model based on clinical characteristics for comparison.

Performance evaluation

Harrell's C-indexes[16] of the DLRN, radiomic signatures, significant clinical characteristics, and clinical model were compared in all cohorts. The confusion matrix of DLRN was also depicted. Moreover, stratification analysis was presented on clinical characteristics and CT scan parameters.

Furthermore, we performed subgroup analysis and calculated pairwise C-indexes on discriminating non-N0 *vs.* N0, N2-3b *vs.* N0-1, N3a-3b *vs.* N0-2, and N3b *vs.* N0-3a. The calibration curve was plotted to assess the calibration of the DLRN on the subgroup analysis. Among the subgroup analysis, non-N0 *vs.* N0 is of special concern since it may determine the surgical strategy for lymphadenectomy. Decision curve analysis was conducted to evaluate the clinical usefulness of our DLRN in guiding lymphadenectomy by quantifying the net benefits.

We further validated our DLRN on the Italian cohort using the Spearman correlation coefficient and overall C-index. Besides, we evaluated the association between DLRN score and overall survival (OS) in the follow-up LAGC cohort using Kaplan–Meier curves.

Statistical analysis

Statistical analysis was conducted with R software (version 3.5.0;

http://www.Rproject.org) and MATLAB. A two-sided $p<0.05$ was used as the criterion of statistically significant difference. In the univariate analysis, the differences in clinical characteristics between the patients in different groups were assessed using independent t-test or Mann–Whitney U test for continuous variables and Fisher exact test or chi-square test for categorical variables. Analysis of variance (ANOVA) and Kruskal–Wallis H test were implemented for comparing three or more groups.

Results

Chi-square test and t-test showed that there was no significant difference in gender or age between PC and VCs in China ($p>0.05$) except for patients' age in the VC2 ($p=0.0040$). As shown in Table S1, the pathologic N stage was significantly associated with tumor size, clinical N stage, clinical T stage, gender, and CA19-9 in the PC ($p<0.05$).

During the radiomic signature building step (Supplementary A6 and Figure S1), SVM was optimally selected to build three radiomic signatures, including arterial signature (6 features), venous signature (6 features), and unenhanced signature (7 features). The final features are shown in Table S3 and Supplementary A6.

The multivariable linear regression analysis in the PC showed that arterial signature, venous signature, and clinical N stage were independent predictors for pathologic N stage (Table S4), while the clinical T stage, tumor size, gender, and CA19-9 were removed. These predictors were combined into the DLRN (Figure 3A). The NRI analysis revealed that the addition of an unenhanced signature into DLRN did not show significantly better performance (NRI 0.0482; $p=0.1870$).

As shown in Figure 3B, there was a significant positive correlation between DLRN score and pathologic N stage, which was also confirmed by the Spearman correlation coefficients (0.626-0.718, $p<0.0001$) in Table S5 and the confusion matrixes in Figure S2. As shown in Table 1, the DLRN showed a good discrimination of N stages in PC (overall C-index 0.821, 95% CI: 0.785-0.858), VC1 (0.777, 0.735-0.819), VC2 (0.817, 0.775-0.860) and VC3 (0.787, 0.737-0.838). Moreover, the DLRN performed significantly better than the clinical N stage, tumor size, and the

clinical model (Table S4) on all the external VCs in China with $p<0.05$. The stratification analysis showed that the performance of our DLRN was not affected by the age, gender, Lauren type, tumor location, the version of CT system, and slice thickness (Figure S3 and Supplementary A7).

The calibration curves of the subgroup analysis showed good agreement between the DLRN predicted outcomes and the real N stages (Figure 3C). Moreover, the DLRN could well discriminate non-N0 from N0 groups in all cohorts (C-indexes: 0.777-0.821, Table S5). If we use this model to guide lymphadenectomy (non-N0 patients receive lymphadenectomy and N0 patients do not), as shown in Figure 3D, the decision curves indicated that the DLRN could add more benefit to patients than single signatures, clinical model, none-lymphadenectomy scheme, and all-lymphadenectomy scheme.

Clinicians may be interested in how many patients with CT-diagnosed N0 disease will be upstaged with DLRN (non-N0 by pathology). These cases could be named as occult LNM, which are with no typical CT signs (i.e., enlarged lymph node). The experimental results showed that DLRN could well detect these patients with occult LNM (81.7% [76/93] upgraded).

We further validated our DLRN on the non-Asian cohort IVC (Table S6). The DLRN also showed good discrimination of N stage in IVC (overall C-index 0.822, 95% CI: 0.756-0.887).

We evaluated the prognostic value of DLRN in the follow-up LAGC cohort (Table S6). The DLRN yielded a predictive accuracy for OS (C-index 0.646, 95% CI: 0.596-0.696, $p<0.0001$). Patients with high DLRN score displayed worse OS (per 1 increase; HR 1.982, 95% CI: 1.592-2.467, $p<0.0001$). As shown in Figure 4, the Kaplan-Meier curves divided by the median value of DLRN score were significantly different (log-rank test $p<0.0001$). Further, we performed univariate analysis and multivariate Cox regression on DLRN and clinical characteristics. As shown in Table S7, the DLRN had the highest C-index of predicting OS in the univariate analysis. The Cox regression identified the DLRN and invaded site as the independent

prognostic factors. The final Cox regression model yielded a C-index of 0.656 (95% CI: 0.606-0.705).

Discussion

This study was an international multi-center collaboration aimed at predicting the number of LNM in LAGC. Our DLRN showed high predictive ability and reproducibility across different centers. Moreover, the ROI segmentation and DLRN score calculation require less than 5 additional minutes per patient during a normal reporting session, which makes DLRN an easy-to-use tool for clinicians. We have already uploaded the model and several examples of CT images on our website http://www.radiomics.net.cn/platform.html as well as on Zenodo https://doi.org/10.5281/zenodo.3701430 for open access.

According to the latest TNM staging system, regional LNs with enlarged short-axis diameter $\geqslant$1 cm and other abnormal signs on imaging are suspicious for nodal involvement[5]. However, this standard (the clinical N stage in this study) showed relatively poor performance in our cohorts. In contrast, our DLRN performed significantly better than the routinely used clinical N stage. Moreover, 81.7% of occult LNMs with no typical CT signs (missed by the radiologists) were detected by DLRN, which indicated that our model could be a supplement to current staging scheme.

Our DLRN may help tailor neoadjuvant therapy, lymphadenectomy, or extent of lymphadenectomy in LAGC. There is growing interest in the use of neoadjuvant therapy before surgery for LAGC.[4] Patients with neoadjuvant chemotherapy were proven to have fewer LNMs after surgery than those without[17]. This finding suggests that our preoperative DLRN may be helpful for tailoring neoadjuvant regimens. Moreover, the decision curve analysis showed that using our DLRN to guide lymphadenectomy could provide more benefit to patients than both non-lymphadenectomy and all-lymphadenectomy schemes. Even for patients with lymphadenectomy, there is a long-running debate over which lymphadenectomy extent (D0, D1, or D2) could be beneficial for patients[4,6,18]. Our nomogram is able to

evaluate the number of LNM preoperatively, which could, in turn, assist in choosing the extent of lymphadenectomy.

This study was performed on three tumor ROIs from multi-phase CT images rather than one ROI from a single CT phase. Although the three ROIs showed different shapes and contents, their radiomic signatures were all significantly associated with the pathologic N stages ($p<0.001$). Furthermore, 13 out of 19 selected features in the three signatures were deep learning features, indicating that the DCNNs could extract correlative quantitative representation reflecting the extent of LNM. As shown in Figure S4, the activation maps of DCNN could highlight some regions of the tumors with a large number of LNM, while the same region was suppressed in tumors with small number of LNM. We suspect that the highlighted regions in the activation maps may be relevant to cancer progression. Besides, the global texture features were also adopted in the radiomic signatures, which might reflect the heterogeneity and invasiveness of the tumor. For example, the “gray-level co-occurrence matrix (GLCM) dissimilarity” feature qualifies the global distribution characteristics of gray-level variability in tumor ROI. The feature "GLCM cluster_tendency" tends to emphasize the ROI with significant textural patterns.

Another finding was that our DLRN was significantly associated with the OS of LAGC patients. Previous studies have proven that LAGC patients with different N stages had different prognosis[4]. Our results further validated the association with N stages as well as the prognosis value of our DLRN. Furthermore, we conducted a cross-cancer analysis and transferred our model to a colorectal cancer cohort (n=80). Interestingly, all three radiomic signatures had the potential to discriminate LNM of colorectal cancer (Supplementary A8), indicating that other gastrointestinal cancers might have similar phenotypes with LNM.

Our study has some limitations. First, this study involved a large number of patients from China but a small number of patients from Italy. A further prospective study on other Asian and large-scale non-Asian populations should be investigated. Second, gastric cancer can have different etiology and biology in different countries or races; how this influences our nomogram is still unclear. However, mixing patients

from different countries/races for training may improve the performance of the model. Third, besides CT, endoscopic ultrasonography (EUS) is also recommended for N staging[4]. The combination of EUS and CT may improve N staging accuracy. Fourth, the 2D features in one single slice rather than 3D features were used. Although the operation is more convenient for the radiologist, the 2D segmentation may not be representative of the entire tumor and some features may be affected from 2D *vs.* 3D. Finally, gastric cancer with microsatellite instability (about 10% percentage) is less likely to have LNM but is likely to have enlarged LNs due to immune infiltrate[19] and its contribution in the nomogram should be further investigated.

In conclusion, a deep learning radiomic nomogram had good predictive ability for N staging in LAGC, which could provide basic information for individual diagnosis and treatment in LAGC.

Acknowledgements

We thank Dr. Lambin Philippe and Dr. Henry C Woodruff from the D-Lab, GROW research institute for Oncology, Maastricht University, The Netherlands, for their carefully review of the paper.

Funding

This work was supported by the National Natural Science Foundation of China (91959130, 81971776, 81771924, 81930053, 81771912, 81671682, 81601469, 81701687, 81227901), The National Science Fund for Distinguished Young Scholars (81925023), National Key R&D Program of China (2017YFA0205200, 2017YFC1308700, 2018YFC0910700, 2017YFC1309100, 2017YFC1309101, 2017YFC1309104), the Beijing Natural Science Foundation (L182061, Z180001), and the Youth Innovation Promotion Association CAS (2017175). Francesco Giganti is funded by the UCL Graduate Research Scholarship and the Brahm PhD scholarship in memory of Chris Adams.

Disclosure

The authors declare no conflict of interest.

Author contributions

D.D., M.J.F., L.T., X.H.S., J.B.G, F.G., F.D.C., J.F.J., Z.Y.L., and J.T. conceived and designed the project. R.P.W., X.C., X.X.W., J.F., D.P., F.D.C., W.C.L., and J.L. acquired the data. X.C., X.X.W., J.F., W.C.L., J.L., and L.T. segmented the tumor manually. D.D. and M.J.F. analyzed and interpreted the data. L.Z.Z. and C.E.H inspected the results. All authors were involved in the drafting and reviewing of the manuscript, and approved the final manuscript for submission.

References

1 Bray F, Ferlay J, Soerjomataram I et al. Global cancer statistics 2018: GLOBOCAN estimates of incidence and mortality worldwide for 36 cancers in 185 countries. CA: Cancer J clin, **68**: 394-424 (2018).

2 Shen L, Shan Y, Hu H et al. Management of gastric cancer in Asia: Resource-stratified guidelines. Lancet Oncol, **14**, e535–e547 (2013).

3 Smyth E C, Verheij M, Allum W et al. Gastric cancer: ESMO clinical practice guidelines for diagnosis, treatment and follow-up. Ann Oncol, **27**, v38-v49 (2016).

4 National Comprehensive Cancer Network (NCCN) guidelines. Available online: http://www.nccn.org/ (accessed on 10 Jan 2018).

5 Amin MB, Edge SB, editors. AJCC cancer staging manual. Springer (2017).

6 Schwarz RE, Smith DD. Extended lymph node dissection for gastric cancer: Who may benefit? Final results of the randomized dutch gastric cancer group trial. J Clin Oncol, **22**, 2069-2077 (2004).

7 Kim HJ, Kim AY, Oh ST et al. Gastric cancer staging at multi-detector row CT gastrography: comparison of transverse and volumetric CT scanning. Radiology, **236**, 879-885 (2005).

8 Lambin P, Riosvelazquez E, Leijenaar R et al. Radiomics: Extracting more information from medical images using advanced feature analysis. Eur J Cancer, **48**, 441-446 (2012).

9 Lambin P, Leijenaar RTH, Deist TM et al. Radiomics: The bridge between medical imaging and personalized medicine. Nat Rev Clin Oncol, **14**, 749-762 (2017).

10 Aerts HJ, Velazquez ER, Leijenaar RT et al. Decoding tumour phenotype by noninvasive imaging using a quantitative radiomics approach. Nat Commun, **5**, 4006 (2014).

11 Huang Y, Liang CC, He L et al. Development and validation of a radiomics nomogram for preoperative prediction of lymph node metastasis in colorectal cancer. J Clin Oncol, **34**, 2157-2164 (2016).

12 Dong D, Tang L, Li ZY et al. Development and validation of an individualized nomogram to identify occult peritoneal metastasis in patients with advanced gastric cancer. Ann Oncol, **30**, 431-438 (2019).

13 Peng H, Dong D, Fang MJ et al. Prognostic value of deep learning PET/CT-based radiomics: Potential role for future individual induction chemotherapy in advanced nasopharyngeal carcinoma. Clin Cancer Res, **25**, 4271-4279 (2019).

14 Sano T, Coit DG, Kim HH et al. Proposal of a new stage grouping of gastric cancer for TNM classification: International Gastric Cancer Association staging project. Gastric Cancer, **20**, 217-225 (2017).

15 Huang G, Liu Z, Pleiss G et al. Convolutional Networks with Dense Connectivity. IEEE T Pattern Anal, DOI: 10.1109/TPAMI.2019.2918284 (2019) .

16 Moons KGM, Altman DG, Reitsma JB et al. Transparent reporting of a multivariable prediction model for individual prognosis or diagnosis (TRIPOD): Explanation and elaboration. Ann Intern Med, **162**, W1-W73 (2015).

17 Schuhmacher C, Gretschel S, Lordick F et al. Neoadjuvant chemotherapy compared with surgery alone for locally advanced cancer of the stomach and cardia: European organisation for research and treatment of cancer randomized trial 40954. J Clin Oncol, **28**, 5210-5218 (2010).

18 Degiuli M, Sasako M, Ponti A et al. Randomized clinical trial comparing survival after D1 or D2 gastrectomy for gastric cancer. British Journal of Surgery, **101**, 23-31 (2014).

19 Corso G, Pedrazzani C, Marrelli D et al. Correlation of microsatellite instability at multiple loci with long-term survival in advanced gastric carcinoma. Arch Surg, **144**: 722-727 (2009).

Figure legends

Figure 1. Flowchart of this international multi-center study.

Figure 2. Workflow of DLRN modeling for N staging in LAGC patients.

Figure 3. DLRN and its performance. (A) DLRN with two contrast-enhanced radiomic signatures and clinical N stage. The points of arterial signature, venous signature and clinical N stage are obtained based on the top "points" bar with scale of 0-100. Then, the total point is calculated by summing the three points. The predicted N stage is obtained by mapping the total point to the "total points" bar and the "predicted N stage" bar. (B) Box plots showing patterns of correlation between pathologic N stages and DLRN in PC, VC1, VC2, and VC3. (C) Calibration curves of DLRN in subgroup analysis on discriminating non-N0 vs. N0, N2-3b vs. N0-1, N3a-3b vs. N0-2, and N3b vs. N0-3a. (D) Decision curve analysis for guiding lymphadenectomy using DLRN, arterial signature, venous signature, clinical model, none-lymphadenectomy scheme, and all-lymphadenectomy scheme.

Figure 4. Kaplan-Meier survival curves of OS on the follow-up LAGC cohort.

Table legends

Table 1. Overall C-index of DLRN and other predictors.

The supplementary materials for online only:

Supplementary A1: Patient recruitment

Supplementary A2: CT image acquisition

Supplementary A3: Radiomic feature extraction

Supplementary A4: Method of radiomic feature selection and signature building

Supplementary A5: Simulated slice thickness dataset building

Supplementary A6: Results of radiomic signature building

Supplementary A7: Stratification analysis

Supplementary A8: Cross-cancer analysis on a colorectal cancer cohort

Figure S1. Heatmaps of radiomic feature expressions.

Figure S2. Confusion matrixes for DLRN.

Figure S3. Box plots showing patterns of correlation between pathologic N stages and DLRN score in stratification analysis.

Figure S4. The diagram of N stages and DCNN activation maps.

Figure S5. ROC curves for the three radiomic signatures to determine LNM vs. non-LNM on the colorectal cancer cohort.

Table S1. Characteristics of patients in the PC and VCs for pathologic N stage groups.

Table S2. The CT image acquisition parameters of the six centers.

Table S3. Input features of the three radiomic signatures.

Table S4. Construction of DLRN and clinical model via multivariable linear regression analysis.

Table S5. Performances of the DLRN in PC and VCs.

Table S6. Characteristics of patients in the IVC and the follow-up LAGC cohort.

Table S7. Results of survival analysis for characteristics and models.

Table 1. Overall C-index of DLRN and other predictors.

	PC	VC1	VC2	VC3	All VCs
DLRN	0.821 (0.785-0.858)	0.777 (0.735-0.819)	0.817 (0.775-0.860)	0.787 (0.737-0.838)	0.797 (0.771-0.823)
Arterial signature	0.766 (0.719-0.812)	0.738 (0.688-0.787)	0.761 (0.704-0.818)	0.716 (0.652-0.780)	0.738 (0.705-0.770)
Venous signature	0.785 (0.744-0.826)	0.719 (0.667-0.770)	0.732 (0.676-0.789)	0.739 (0.678-0.799)	0.739 (0.708-0.770)
Unenhanced signature	0.782 (0.740-0.824)	0.729 (0.681-0.776)	0.676 (0.611-0.740)		0.697 (0.657-0.736)*
Clinical N stage	0.679 (0.629-0.730)	0.685 (0.629-0.741)	0.698 (0.631-0.766)	0.709 (0.619-0.800)	0.705 (0.669-0.742)
Clinical model	0.689 (0.642-0.736)	0.652 (0.593-0.711)	0.671 (0.605-0.737)	0.732 (0.661-0.804)	0.675 (0.638-0.713)
Tumor size	0.666 (0.619-0.714)	0.666 (0.610-0.722)	0.673 (0.616-0.730)	0.638 (0.565-0.711)	0.664 (0.630-0.699)

Note. * the value was calculated based on VC1 and VC2.

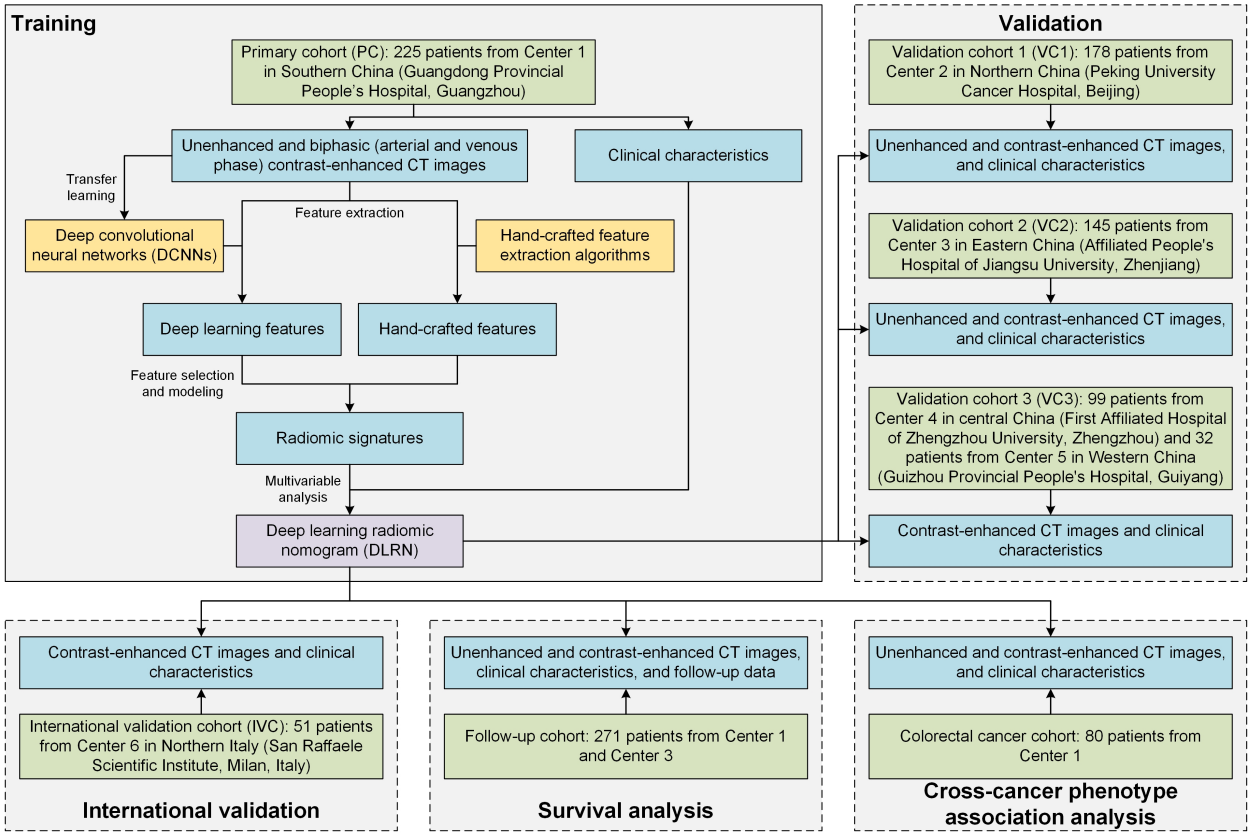

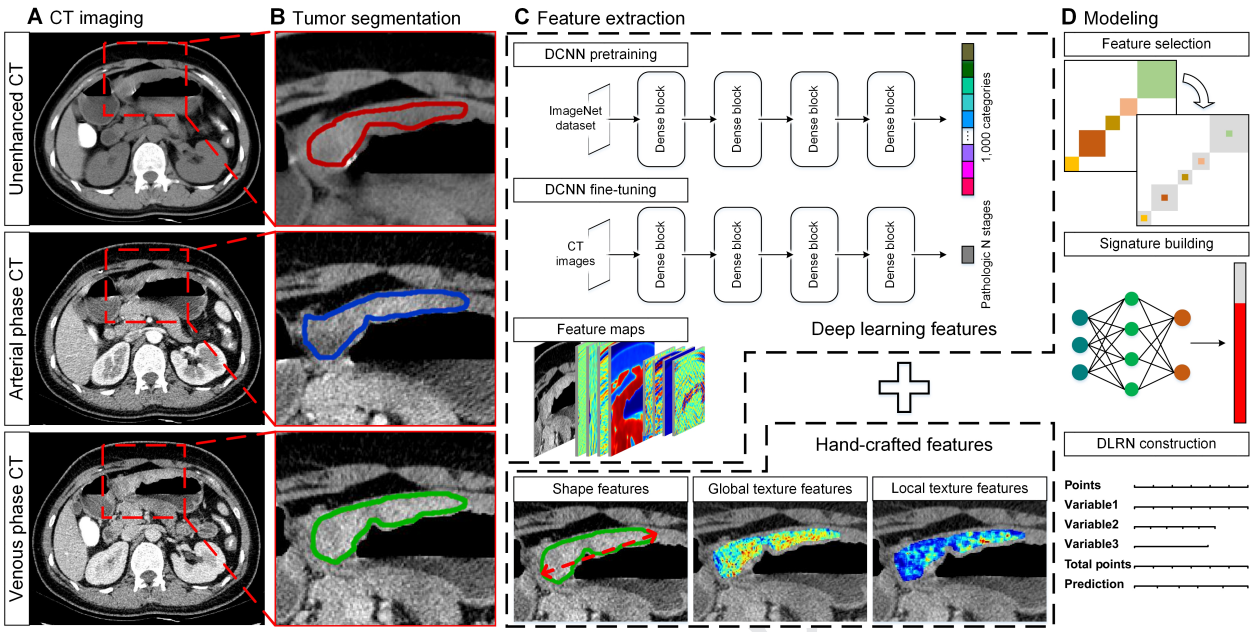

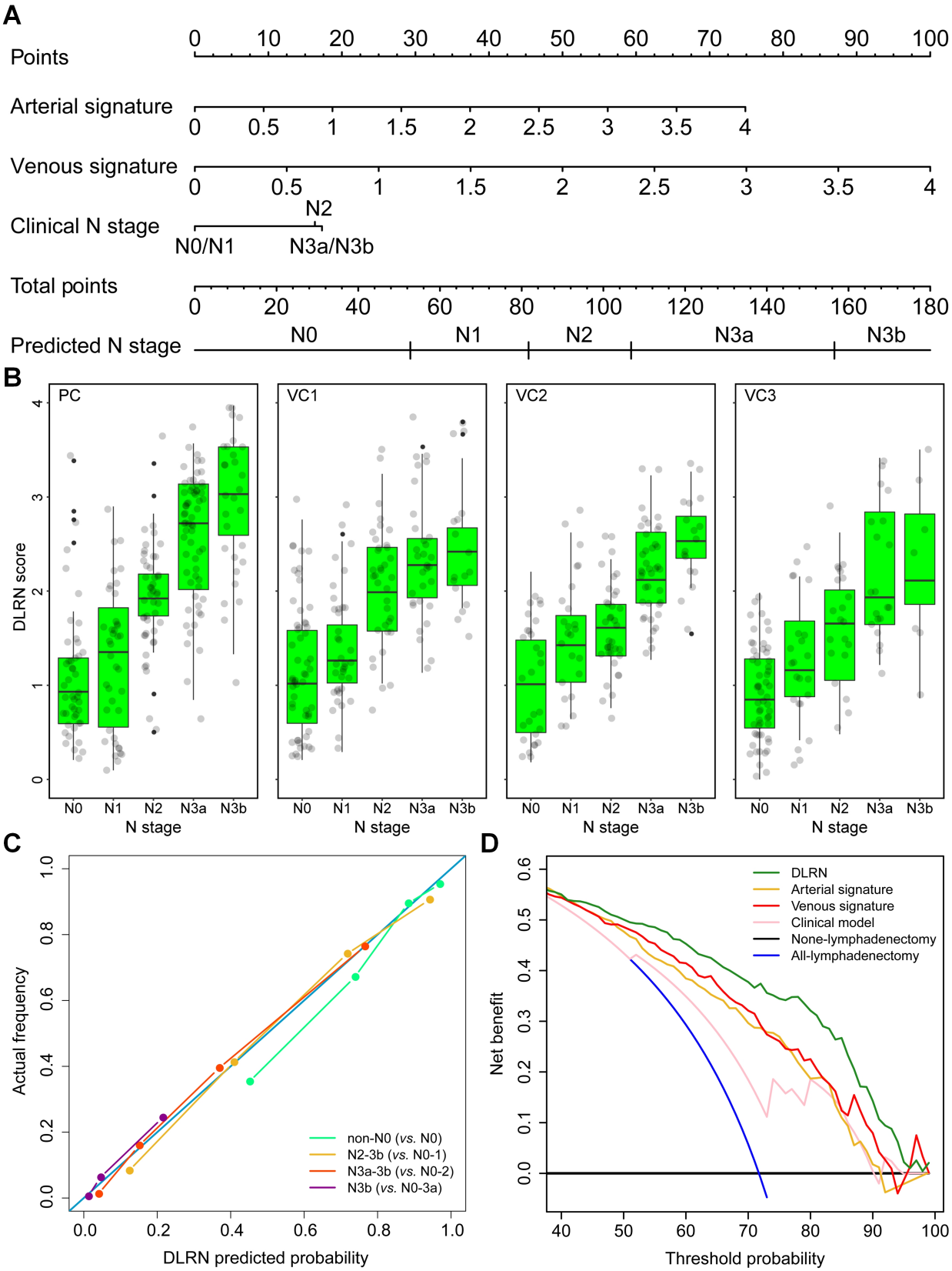
A
Points
0 10 20 30 40 50 60 70 80 90 100
Arterial signature
0 0.5 1 1.5 2 2.5 3 3.5 4
Venous signature
0 0.5 1 1.5 2 2.5 3 3.5 4
Clinical N stage
N2
N0/N1
N3a/N3b
Total points
0 20 40 60 80 100 120 140 160 180
Predicted N stage
N0
N1
N2
N3a
N3b
B
PC
VC1
VC2
VC3
DLRN score
N0 N1 N2 N3a N3b
N stage
C
Actual frequency
DLRN predicted probability
non-N0 (vs. N0)
N2-3b (vs. N0-1)
N3a-3b (vs. N0-2)
N3b (vs. N0-3a)
D
Net benefit
Threshold probability
DLRN
Arterial signature
Venous signature
Clinical model
None-lymphadenectomy
All-lymphadenectomy

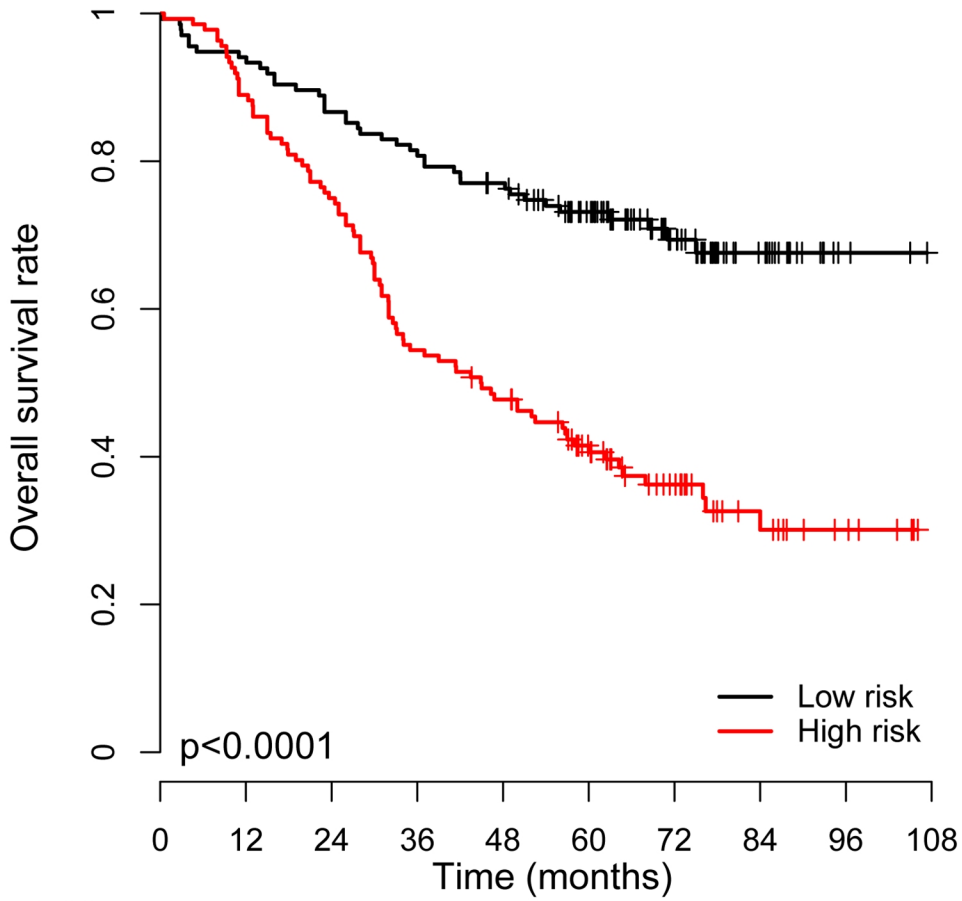

Number at risk

Low risk	135	127	117	110	102	81	44	21	3	0
High risk	136	121	102	74	64	46	27	13	6	0